Hyperfine Sublevel Correlation (HYSCORE) Spectra for Paramagnetic Centers with Nuclear Spin $I = 1$ Having Isotropic Hyperfine Interactions†

Alexander G. Maryasov*,‡,§ and Michael K. Bowman§

Institute of Chemical Kinetics and Combustion SB RAS, Novosibirsk 630090, Russia, and W. R. Wiley Environmental Molecular Sciences Laboratory, Pacific Northwest National Laboratory, Richland, Washington 99352-0999

Received: April 7, 2003; In Final Form: October 22, 2003

Hyperfine sublevel correlation (HYSCORE) spectra of paramagnetic centers that have nuclei with nuclear spin $I = 1$ and isotropic hyperfine interactions (HFIs) and arbitrary nuclear quadrupole interactions (NQIs) are shown to consist of ridges that have zero width. A parametric presentation of these ridges is suggested that shows the range of possible frequencies in the HYSCORE spectrum and aids in spectral assignments and rapid estimation of spin Hamiltonian parameters. An alternative approach for the spectral density calculation is presented. This methodology is based on spectral decomposition of the Hamiltonian and requires only the eigenvalues. An atlas of HYSCORE spectra is given in the Supporting Information for this paper. This approach is applied to the estimation of the spin Hamiltonian parameters of the oxovanadium−EDTA complex.

Introduction

The pulsed electron paramagnetic resonance (EPR) technique is widely used to investigate the structure of molecules that contain paramagnetic centers (PCs) or labeled with appropriate spin labels. The hyperfine interactions (HFIs) of unpaired electrons with surrounding nuclei lead to the appearance of quantum beats in the system response to microwave (mw) pulses. In the case of electron spin−echo (ESE), these beats are called ESE envelope modulation (ESEEM).[1] The frequency spectrum of such modulations contains information about the system Hamiltonian parameters and can be used to draw valid conclusions about the structure of the system in question.

Several variations of the ESE technique are used to obtain two-dimensional (2-D) modulation spectra.[2] The use of two dimensions leads to better resolution and easier interpretation of the data by separating overlapping lines and by correlating frequencies to aid spectral assignment. The most widely used 2-D method is HYSCORE (HYperfine Sublevel COrRElation) spectroscopy.[3] It applies a four-pulse sequence to the system

$$\left(\frac{\pi}{2}\right)_1 - \tau - \left(\frac{\pi}{2}\right)_2 - t_1 - (\pi)_3 - t_2 - \left(\frac{\pi}{2}\right)_4 - \tau - \text{echo} \quad (1)$$

accompanied by phase cycling to remove additional unwanted echoes and free induction decay signals. The signal measured is the stimulated echo signal produced by the action of pulses 1, 2, and 4, as a function of times t_1 and t_2. The third pulse causes an electron spin flip, which produces a correlation of the nuclear hyperfine frequencies from different electron spin manifolds. In the simplest case of electron spin $S = {}^1/_2$ and nuclear spin $I = {}^1/_2$, there is a straightforward graphical algorithm that rapidly provides the hyperfine values.[4,5] In the more-complex situation of nuclear spins $I \geq 1$ that have significant quadrupolar interactions, only numerical simulation has been used for detailed analysis in noncrystalline samples.[6−8]

Systems with $I = 1$ and significant quadrupolar coupling, such as ^{14}N and ^{2}H, are widespread and are important in biology, chemistry, and materials science. This contribution is devoted to the analysis of HYSCORE spectra for a $S = {}^1/_2$ and $I = 1$ system with arbitrary quadrupolar interaction and isotropic nuclear hyperfine and Zeeman interactions. This treatment is based on the exact solution of the $I = 1$ spin Hamiltonian[9,10] and its spectral presentation using the Cayley−Hamilton theorem.[11,12]

Theory

The HYSCORE Signal in the Case of Arbitrary Nuclear Spin. In an earlier paper,[13] we developed a recurrence relation for the echo signals as a function of the number of applied mw pulses. Applying this to the four-pulse sequence (sequence 1), the following expression may be obtained for the time course of the HYSCORE echo signal:

$$V(t'') = A \exp(\iota\delta\omega t'')\mathrm{Tr}[\hat{N}(-\tau - t'') \times \{\hat{K}_\beta(-t_2)\hat{K}_\alpha(-t_1)\hat{N}(\tau)\hat{K}_\alpha(t_1)\hat{K}_\beta(t_2) + \hat{K}_\alpha(-t_2)\hat{K}_\beta(-t_1)\hat{N}(\tau)\hat{K}_\beta(t_1)\hat{K}_\alpha(t_2)\}] \quad (2)$$

Here, the trace is taken over nuclear spins, A is an instrumental echo amplitude scaling factor, $\delta\omega$ is the difference of the resonance frequency of the PC in question and the frequency of mw pulses, and the time t'' is measured from the maximum of the echo signal ($t'' = t - (t_1 + t_2 + 2\tau)$). The operators $\hat{K}_m$ are nuclear subsystem propagators for each electron spin manifold, where m denotes the eigenstate (α or β) throughout this paper:

$$\hat{K}_m(t) = \exp\{\iota t\hat{H}_{I,m}\} \quad (3)$$

The nuclear spin I sub-Hamiltonians are written (all quantities

† Part of the special issue "Jack H. Freed Festschrift".

* Author to whom correspondence should be addressed. E-mail address: maryasov@ns.kinetics.nsc.ru.

‡ Institute of Chemical Kinetics and Combustion, SB RAS.

§ Pacific Northwest National Laboratory.

10.1021/jp034912+ CCC: $27.50
Published on Web 03/19/2004

in units of radians per second), in the laboratory frame, as

$$H_{I\alpha(\beta)} = \left(\omega_I \pm \frac{a}{2}\right)\hat{I}_z + \hat{\vec{I}}\,\vec{\vec{Q}}\,\hat{\vec{I}} \tag{4}$$

with ω_I, a, and $\vec{\vec{Q}}$ being the nuclear Zeeman frequency, the hyperfine coupling constant, and the quadrupolar interaction tensor, respectively. The modulation operator $\hat{N}$ is used in eq 2 for compact presentation:

$$\hat{N}(t) = \hat{K}_\alpha(-t)\hat{K}_\beta(t) \tag{5}$$

Equation 2 is obtained in the limit of hard pulses that excite the entire EPR spectrum of the PC. All unwanted signals are assumed to be removed by means of appropriate phase cycling.

Equation 2 may be rewritten to give the echo intensity, measured at its maximum value at $t'' = 0$:

$$V' = \mathrm{Tr}[\hat{K}_\alpha(-t_1)\hat{N}(\tau)\hat{K}_\alpha(t_1)\hat{K}_\beta(t_2)\hat{N}(-\tau)\hat{K}_\beta(-t_2)] + \mathrm{Tr}[\hat{K}_\beta(-t_1)\hat{N}(\tau)\hat{K}_\beta(t_1)\hat{K}_\alpha(t_2)\hat{N}(-\tau)\hat{K}_\alpha(-t_2)] \tag{6}$$

Here, $V' = V/A$. The equality $\mathrm{Tr}(\hat{A}\hat{B}) = \mathrm{Tr}(\hat{B}\hat{A})$ was used to transform eq 2. The two terms on the right-hand side of eq 6 are related to each other by an interchange of their indexes, $\alpha \Leftrightarrow \beta$.

In the case that several nuclei interact with the PC, the product rule must be applied separately to each term on the right-hand side of eq 6. If we define operators $\hat{Z}_m(\tau,t)$ as

$$\hat{Z}_m(\tau,t) = \hat{K}_m(-t)\hat{N}(\tau)\hat{K}_m(t) \tag{7}$$

eq 6 may be simplified:

$$V' = \mathrm{Tr}[\hat{Z}_\alpha(\tau,t_1)\hat{Z}_\beta(-\tau,-t_2) + \hat{Z}_\beta(\tau,t_1)\hat{Z}_\alpha(-\tau,-t_2)] \tag{8}$$

The operators $Z_{\alpha(\beta)}$ describe the evolution of the nuclear modulation operator (eq 5) under the influence of the nuclear spin Hamiltonian belonging to different electron spin manifolds. The $Z_{\alpha(\beta)}$ operators have a clear physical interpretation in the limit of short τ, when the modulation operator (eq 5) may be approximated as

$$\hat{N}(\tau \to 0) = 1 - \imath\tau a\hat{I}_z \tag{9}$$

to give

$$\hat{Z}_m(\tau \to 0,t) = 1 - \imath a\tau\hat{J}_{zm}(t) \tag{10}$$

Here, the operators J describe the evolution of the projection of the initial nuclear magnetization onto the hyperfine field under the action of the nuclear spin sub-Hamiltonians for different electron spin manifolds:

$$\hat{J}_{zm}(t) = \hat{K}_m(-t)\hat{I}_z\hat{K}_m(t) \tag{11}$$

When the nuclear quantization axis coincides with the direction of the hyperfine field, $\hat{J}_{zm}(t)$ is a constant and no modulation occurs.

HYSCORE spectra are rarely measured in this short τ limit. However, for comparison of simulated spectra, it is convenient to calculate spectra in the short τ limit, where the so-called "τ suppression effect" does not occur, rather than at some larger value of τ, where some spectral features may vanish. The calculated spectra presented here will use this short τ approximation; however, all other calculations are valid for all finite values of τ.

In the case of nuclear spin $I = {}^1/_2$, it was possible to construct a vector model for ESEEM phenomena.[13] Unfortunately, the motion of $I = 1$ with finite quadrupolar coupling is more complex and not easily visualized. One must find the eigensystem of the Hamiltonian (eq 4) to calculate nuclear propagators, whether using the aforementioned outlined formalism or the traditional approach of Mims. Although numerical solutions of the eigensystem are commonly used, an analytical solution was developed in a series of papers by Muha.[9,10] The eigenvectors of the nuclear Hamiltonian allow calculation of the Mims matrix M, whose elements are used together with the eigenvalues in conventional calculations of HYSCORE spectra.[3,14]

Here, we present an alternative approach that is based on the Cayley−Hamilton theorem and on the spectral decomposition of linear operators, where only the eigenvalues of the Hamiltonian are needed to calculate projection operators onto the Hamiltonian eigenstates[11,12] for the calculation of HYSCORE spectra. It is broadly applicable to other forms of coherent spectroscopy and to HYSCORE spectra from any general nuclear spin Hamiltonian, although we explicitly consider $I = 1$ with nuclear quadrupole interactions (NQIs), Zeeman interactions, and isotropic HFIs. This approach results in highly efficient calculation of the spectra and provides considerable insight into the form of HYSCORE spectra and their detailed interpretation.

Analysis of the Nuclear Hamiltonian. The Hamiltonian (eq 4) has its simplest form in the principal axis frame, (X,Y,Z), of the quadrupolar interaction, where

$$H_{I,m} = \kappa\{[3\hat{I}_Z{}^2 - I(I+1)] + \eta(\hat{I}_X{}^2 - \hat{I}_Y{}^2)\} + \vec{D}_m\cdot\hat{\vec{I}} \tag{12}$$

Here, κ is the quadrupolar coupling constant, η the asymmetry parameter, and $\vec{D}_m$ the sum of the external magnetic field and the hyperfine field, in the nuclear quadrupole frame

$$\vec{D}_m = D_m\{\sin\theta\cos\phi, \sin\theta\sin\phi, \cos\theta\} \tag{13}$$

Here, θ and ϕ are the polar and azimuthal angles that denote the orientation of the external magnetic field in the frame, and

$$D_m = \omega_I \pm \frac{a}{2} \tag{14}$$

The secular equation for $I = 1$ in each electron spin manifold is

$$\Omega_m^3 + p_m\Omega_m - q_m = 0 \tag{15}$$

The coefficients are readily expressed in terms of the invariants of the Hamiltonian, as

$$p_m = -\frac{1}{2}\mathrm{Tr}(H_{I,m}^2) \tag{16}$$

$$q_m = \frac{1}{3}\mathrm{Tr}(H_{I,m}^3) \tag{17}$$

whose explicit forms are

$$p_m = -[D_m^2 + \kappa^2(3+\eta^2)] \tag{18}$$

$$q_m = \kappa D_m^2 f(\eta,\theta,\phi) - 2\kappa^3(1-\eta^2) \tag{19}$$

with

$$f(\eta,\theta,\phi) = \cos^2\theta + \cos 2\theta + \eta\sin^2\theta\cos 2\phi \tag{20}$$

The solution of eq 15 gives the eigenvalues[9,10]

$$\Omega_{m,j} = \left(\frac{4|p_m|}{3}\right)^{1/2} \cos\left(\frac{\lambda_m + 2\pi j}{3}\right) \tag{21}$$

for $j = 0$, 1, 2, and

$$\cos \lambda_m = \left(\frac{3}{|p_m|}\right)^{3/2}\left(\frac{q_m}{2}\right) \tag{22}$$

The right-hand side of eq 22 always lies between -1 and 1, so that the eigenvalues are real quantities for all values of the Hamiltonian parameters. Let us note that the eigenvalues (eq 21) are dependent on D_m^2. This means that the exchange of parameters

$$\frac{a}{2} \leftrightarrow \omega_I \tag{23}$$

does not alter the eigenvalues of the nuclear subensembles, although it will alter the eigenvectors. The practical consequence of this fact will be illustrated later in the paper.

The transition frequencies between the jth and kth levels (eq 21) in the same manifold are

$$\Omega_m^{j,k} = \Omega_{m,j} - \Omega_{m,k} = 2|p_m|^{1/2} \operatorname{sign}[k - j]\xi_{m,j+k} \tag{24}$$

where the dimensionless factor

$$\xi_{m,n} = \sin\left(\frac{\lambda_m + \pi n}{3}\right) \tag{25}$$

is introduced. The index is uniquely determined ($n = 1, 2, 3$), because transitions must be between different levels so that $j \neq k$ in eq 24.

Analysis of the Transition Frequencies

The most important feature of the nuclear Hamiltonian with isotropic HFI is that the dependence of the eigenvalues (eq 21) and the transition frequencies (eqs 24, 25) on the orientation of the external magnetic field is confined to the parameter f in eq 20. The range of this parameter is

$$-(1 + \eta) \leq f \leq 2 \tag{26}$$

as θ and ϕ are varied independently through their own ranges. Such a dependence allows us to relate the transition frequency in one electron spin manifold with that in the other manifold without explicit attention to the orientation of the external magnetic field in the nuclear quadrupole frame. In the case of anisotropic HFI, D_m becomes orientation-dependent, as do p_m and q_m.

Let us consider the properties of the factor ξ in eq 25 as functions of f and n. The quantity λ_m is dependent on f monotonically, because arccos(x) is a monotonic function of its argument inside the interval $0 \leq \lambda_m \leq \pi$. This means that $\xi_{m,2}$ and $\xi_{m,3}$ are also monotonic functions of f, because the argument of the sine in eq 24 may vary between $2\pi/3$ and π in the case of $\xi_{m,2}$ and between π and $4\pi/3$ in the case of $\xi_{m,3}$. In the case of $\xi_{m,1}$ the sine argument may vary between $\pi/3$ and $2\pi/3$ and provide a maximum value of 1 when $\lambda_m = \pi/2$. We can consequently arrange the relative values of these factors

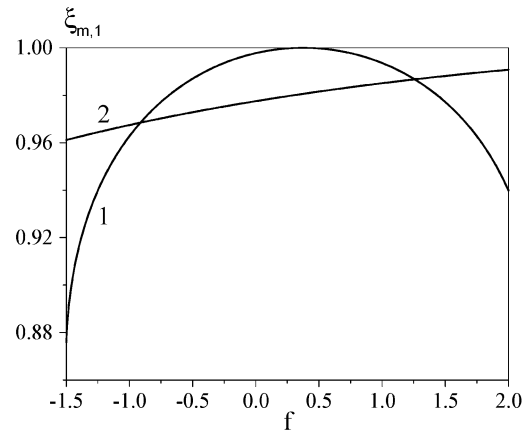

Figure 1. Dependence of the double quantum transition frequency factor ξ on the parameter f. Curves 1 and 2 respectively correspond to the weak and strong quadrupole conditions of eq 30. The following parameter values were used for the calculations: $\eta = 0.5$, $D_m/\kappa = 2$ (for curve 1), and $D_m/\kappa = 0.5$ (for curve 2).

(and respective transition frequencies) as follows:

$$1 \geq \xi_{m,1} \geq \frac{\sqrt{3}}{2} \geq \xi_{m,2} \geq 0 \geq \xi_{m,3} \geq -\frac{\sqrt{3}}{2} \tag{27}$$

Relation 27 shows that $\xi_{m,1}$ has the largest absolute value and produces the so-called "double quantum nuclear transition" in the mth manifold, whereas the other two frequencies correspond to the single quantum transitions.

Making use of relations 22 and 26, one can easily find the minimum and maximum values of λ_m:

$$\lambda_m^{\max} = \arccos\left[-\left(\frac{3}{|p_m|}\right)^{3/2}\frac{\kappa D_m^2(1 + \eta) + 2\kappa^3(1 - \eta^2)}{2}\right] \tag{28}$$

$$\lambda_m^{\min} = \arccos\left\{\left(\frac{3}{|p_m|}\right)^{3/2}[\kappa D_m^2 - \kappa^3(1 - \eta^2)]\right\} \tag{29}$$

Here, we assume that $\kappa > 0$, so that $\lambda_m^{\max} > \pi/2$. If $\kappa < 0$, the max and min labels are exchanged. In either case, for the point $\pi/2$ to be contained between $\lambda_m^{\min}$ and $\lambda_m^{\max}$, the following relationship is required:

$$D_m^2 > \kappa^2(1 - \eta^2) \tag{30}$$

in which case the maximum value of the factor $\xi_{m,1} = 1$ occurs at

$$f_m = \frac{2\kappa^2(1 - \eta^2)}{D_m^2} \tag{31}$$

Interestingly, note that, for $\eta = 1$, the double quantum transitions in both manifolds have their maximum values of $2\sqrt{|p_\alpha|}$ and $2\sqrt{|p_\beta|}$ at the same value of $f = 0$. Examples of the dependence of $\xi_{m,1}$(f) are shown in Figure 1. The relationship depicted in expression 30 defines a "weak quadrupole" condition and a "strong quadrupole" condition.

The HYSCORE Spectrum in an Orientationally Disordered System

We can now present an alternative way to calculate the 2-D spectrum of the HYSCORE signal from the eigenvalues, based

on the spectral decomposition of a linear operator, in terms of the projection operators.

The $\hat{P}_{m,n}$ projection operators for the Hamiltonian eigenstates (eq 12) are related to the eigenvalues as[11,12]

$$\hat{P}_{\alpha,n} = \prod_{j \neq n} \frac{\hat{H}_{I,\alpha} - \hat{1}\Omega_{\alpha,j}}{\Omega_{\alpha,n} - \Omega_{\alpha,j}} \tag{32a}$$

$$\hat{P}_{\beta,n} = \prod_{j \neq n} \frac{\hat{H}_{I,\beta} - \hat{1}\Omega_{\beta,j}}{\Omega_{\beta,n} - \Omega_{\beta,j}} \tag{32b}$$

Here, $n, j = 0, 1, 2$ and $\hat{1}$ is used as the unity operator in the nuclear spin subspace. For $I = 1$, these are 3×3 matrixes and may be written as

$$\hat{P}_{\alpha,n} = \frac{\hat{H}_{I,\alpha}^2 + \hat{H}_{I,\alpha}\Omega_{\alpha,n} + \hat{1}q_\alpha\Omega_{\alpha,n}^{-1}}{3q_\alpha\Omega_{\alpha,n}^{-1} - 2p_\alpha} \tag{33a}$$

$$\hat{P}_{\beta,n} = \frac{\hat{H}_{I,\beta}^2 + \hat{H}_{I,\beta}\Omega_{\beta,n} + \hat{1}q_\beta\Omega_{\beta,n}^{-1}}{3q_\beta\Omega_{\beta,n}^{-1} - 2p_\beta} \tag{33b}$$

Equations 32−33 are valid in the absence of degeneracy in the Hamiltonian eigensystem, which is always the case, except when the magnetic field is oriented along the *Z*-axis of the nuclear quadrupole frame with $\eta \equiv 0$ or when an accidental degeneracy occurs.

Now it is possible to express the propagators (eq 3) for nuclear spins, in terms of the projection operators (eq 33):

$$\hat{K}_m(t) = \sum_n \hat{P}_{m,n} \exp\{\imath t\Omega_{m,n}\} \tag{34}$$

The HYSCORE signal (eq 6) becomes

$$V' = \sum_{n,j,r,s} \exp\{\imath t_1(\Omega_{\alpha,j} - \Omega_{\alpha,n}) + \imath t_2(\Omega_{\beta,r} - \Omega_{\beta,s})\}A_{njrs}(\theta,\phi) + \sum_{n,j,r,s} \exp\{\imath t_1(\Omega_{\beta,j} - \Omega_{\beta,n}) + \imath t_2(\Omega_{\alpha,r} - \Omega_{\alpha,s})\}B_{njrs}(\theta,\phi) \tag{35}$$

with

$$A_{njrs}(\theta,\phi) = \mathrm{Tr}[\hat{P}_{\alpha,n}\hat{N}(\tau)\hat{P}_{\alpha,j}\hat{P}_{\beta,r}\hat{N}(-\tau)\hat{P}_{\beta,s}] \tag{36}$$

$$B_{njrs}(\theta,\phi) = \mathrm{Tr}[\hat{P}_{\beta,n}\hat{N}(\tau)\hat{P}_{\beta,j}\hat{P}_{\alpha,r}\hat{N}(-\tau)\hat{P}_{\alpha,s}] \tag{37}$$

or, in the small τ limit (eq 9),

$$A_{njrs}(\theta,\phi) = a^2\tau^2\mathrm{Tr}[\hat{P}_{\alpha,n}\hat{I}_z\hat{P}_{\alpha,j}\hat{P}_{\beta,r}\hat{I}_z\hat{P}_{\beta,s}] \tag{38}$$

$$B_{njrs}(\theta,\phi) = a^2\tau^2\mathrm{Tr}[\hat{P}_{\beta,n}\hat{I}_z\hat{P}_{\beta,j}\hat{P}_{\alpha,r}\hat{I}_z\hat{P}_{\alpha,s}] \tag{39}$$

The *A* and *B* factors in eq 35 are identical to those in the conventional matrix formulation of HYSCORE. However, here, they are expressed in terms of the Hamiltonian and its eigenvalues, rather than in terms of the eigenvectors in the Mims matrix *M* of the conventional description.[3]

We will now obtain the spectral density of the signal following our earlier procedure,[15] where Fourier transformation is applied before integration of the signal over orientations of the system. Two-dimensional Fourier transformation of eq 35,

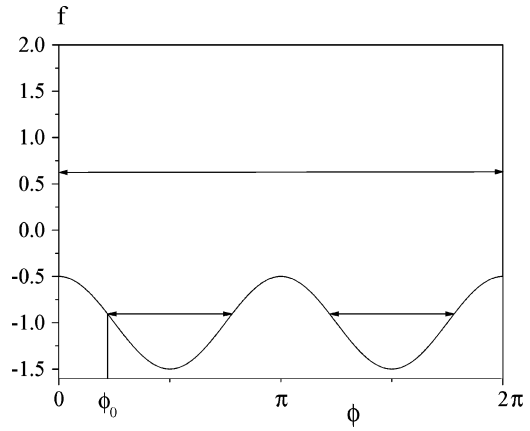

Figure 2. Region of integration for variables *f* and ϕ. The value $\eta = 0.5$ was used for this example. The position of the point ϕ_0 for some particular value of *f* (see eq 50 in the text) is also shown.

with respect to times t_1 and t_2, gives

$$V'_F(\theta,\phi) = \sum_{n,j,r,s} \delta(\omega_1 - \Omega_{\alpha,j} + \Omega_{\alpha,n})\delta(\omega_2 - \Omega_{\beta,r} + \Omega_{\beta,s})A_{njrs}(\theta,\phi) + \sum_{n,j,r,s} \delta(\omega_1 - \Omega_{\beta,j} + \Omega_{\beta,n})\delta(\omega_2 - \Omega_{\alpha,r} + \Omega_{\alpha,s})B_{njrs}(\theta,\phi) \tag{40}$$

Here, $\delta(x)$ is the Dirac δ-function, and ω_i are the frequency conjugates of the times t_i, for $i = 1, 2$. There are ridges located along both axes when $j = n$ or $r = s$ but they are generally suppressed during data processing and will not be considered explicitly here.

The product of two δ-functions on the right-hand side of eq 40 and the dependence of the eigenvalues $\Omega_{m,j}$ on a single argument *f* leads to the retention of one δ-function on the right-hand side after signal integration. This means that the 2-D spectrum in the case of isotropic HFI is a set of zero-width ridges (ZWRs), regardless of the symmetry of the quadrupole interaction, unlike the case for anisotropic HFI that was reported previously.[3]

To find the HYSCORE spectrum of an orientationally disordered system, one must integrate eq 40 over a hemisphere of all possible orientations of the external magnetic field:

$$\bar{V}_F = 2 \iint\limits_{\substack{0 \le \phi \le 2\pi \\ 0 \le \cos\theta \le 1}} V'_F(\theta,\phi)\, \mathrm{d}\phi\, \mathrm{d}(\cos\theta) \tag{41}$$

First, we rewrite the integral in terms of *f* and ϕ to simplify the calculations:

$$\bar{V}_F = 2\int\int V'_F(f,\phi)J(f,\phi)\, \mathrm{d}\phi\, \mathrm{d}f \tag{42}$$

where $J(f,\phi)$ is the Jacobian for the transformation to the new integration variables, in this case,

$$J(f,\phi) = \{4(f + 1 - \eta\cos 2\phi)(3 - \eta\cos 2\phi)\}^{-1/2} \tag{43}$$

The region of integration is $0 \le \phi \le 2\pi$ and $-1 + \eta\cos 2\phi \le f \le 2$; it is shown in Figure 2. To complete the transformation, one must substitute

$$\theta = \arccos\left(\frac{f + 1 - \eta\cos 2\phi}{3 - \eta\cos 2\phi}\right)^{1/2} \tag{44}$$

as needed.

Direct calculations of the aforementioned integrals can be performed, but it leads to rather cumbersome relations. That approach must be used in the more-general case of anisotropic HFI. However, in this particular case of isotropic HFI, it is faster to calculate the spectral densities using a parametric presentation of the ZWRs. Let us integrate the A_{njrs} term in eq 40 for the HYSCORE spectrum:

$$\bar{V}_{FA,njrs} = 2\int\int \delta(\omega_1 - \Omega_\alpha^{j,n}(f))\delta(\omega_2 - \Omega_\beta^{r,s}(f))A_{njrs}(f,\phi)J(f,\phi)\,\mathrm{d}\phi\,\mathrm{d}f \quad (45)$$

This term is nonzero only along the ZWR that correlates the $j \rightarrow n$ transition in the α manifold with the $r \rightarrow s$ transition in the β manifold. This ridge may be conveniently described parametrically as a three-dimensional vector $\vec{\boldsymbol{R}}_{\alpha,\beta}^{jn,rs}$, with each component being dependent on a single parameter f:

$$\vec{\boldsymbol{R}}_{\alpha,\beta}^{jn,rs} = \begin{Bmatrix} \Omega_\alpha^{j,n}(f) \\ \Omega_\beta^{r,s}(f) \\ A'_{njrs}(f) \end{Bmatrix} \quad (46)$$

The first two components are a pair of frequencies ω_1 and ω_2, and the third component is the spectral density of the signal correlating those two frequencies:

$$A'_{njrs}(f) = 2Q_A^{njrs}(f)\int_{\{\phi\}(f)} A_{njrs}(f,\phi)J(f,\phi)\,\mathrm{d}\phi \quad (47)$$

Here, the normalization factor Q is introduced. It appears because of the variation in the speed of motion of the point $\{\omega_1,\omega_2\}$ as f is varied

$$Q_A^{njrs}(f) = \left\{\left[\frac{\partial\Omega_\alpha^{j,n}(f)}{\partial f}\right]^2 + \left[\frac{\partial\Omega_\beta^{r,s}(f)}{\partial f}\right]^2\right\}^{-1/2} \quad (48)$$

to provide the actual signal intensity per unit length of the ZWR in the plane. The interval of integration for ϕ is (see also Figure 2)

$$\{\phi\} = 0 \le \phi \le 2\pi \quad (\text{if } -1+\eta \le f \le 2 \text{ and otherwise it consists of two regions})$$
$$= \{\phi_0 \le \phi \le \pi - \phi_0\} \text{ and } \{\pi + \phi_0 \le \phi \le 2\pi - \phi_0\} \quad (\text{if } f < -1+\eta) \quad (49)$$

where

$$\phi_0 = \frac{1}{2}\arccos\left(\frac{f+1}{\eta}\right) \quad (50)$$

The normalization factor may be simplified using eq 24,

$$Q_A^{njrs}(f) = \frac{1}{2}\left\{\left|p_\alpha\right|\left[\frac{\partial\xi_{\alpha,j+n}(f)}{\partial f}\right]^2 + \left|p_\beta\right|\left[\frac{\partial\xi_{\beta,r+s}(f)}{\partial f}\right]^2\right\}^{-1/2} \quad (51)$$

with the derivatives

$$\frac{\partial\xi_{m,n}}{\partial f} = -\frac{\sqrt{3}\kappa D_m^2}{2|p_m|^{3/2}\sin\lambda_m}\cos\left(\frac{\lambda_m + \pi n}{3}\right) \quad (52)$$

so that

$$Q_A^{njrs}(f) = \frac{1}{\sqrt{3}|\kappa|}\left\{D_\alpha^4 p_\alpha^{-2}\sin^{-2}\lambda_\alpha\cos^2\left[\frac{\lambda_\alpha + \pi(n+j)}{3}\right] + D_\beta^4 p_\beta^{-2}\sin^{-2}\lambda_\beta\cos^2\left[\frac{\lambda_\beta + \pi(r+s)}{3}\right]\right\}^{-1/2} \quad (53)$$

with the quantities λ_α and λ_β defined in eq 22. For the ridges that originate from the B terms, the appropriate equations are obtained by the exchange of $\alpha \leftrightarrow \beta$ in the aforementioned equations.

The ZWRs are the peaks and ridges in the HYSCORE spectrum that correlate frequencies from different electron spin manifolds. They form several characteristic patterns that are helpful in an initial analysis. The simplest situation occurs for the ZWR that correlates single quantum transitions in both manifolds, denoted here as C_{11} and also known as an sq,sq correlation:

$$n + j \ge 2 \quad (54a)$$
$$r + s \ge 2 \quad (54b)$$

In this case, both frequencies are monotonic, with respect to f, thus giving a monotonic curve in the plane with extreme values of the frequencies at each end of the curve.

A less-trivial situation is observed when one transition is single quantum and the other is double quantum (C_{12}); this is called an sq,dq or dq,sq correlation:

$$\min(n + j, r + s) = 1 \quad (55a)$$
$$\max(n + j, r + s) \ge 2 \quad (55b)$$

There are two possibilities in this case:

(a) In the case of weak NQI in the electron spin manifold of the double quantum frequency, as defined by the inequality in eq 30, there will be an extreme value ω_{extr} on the interior of the curve. The absolute value of this extreme frequency is

$$|\omega_{\mathrm{extr}}| = 2\sqrt{|p_m|} \quad (56)$$

(b) In the case of strong quadrupoles in the dq frequency manifold, the ridge will be a monotonic curve, as in the case of C_{11}.

The most complex situation occurs when both transitions are double quantum (C_{22}), which is known as a dq,dq correlation:

$$n + j = 1 \quad (57a)$$
$$r + s = 1 \quad (57b)$$

There are three possibilities in this case:

(a) Strong NQI are present in both manifolds, which produces a monotonic curve, as observed for C_{11} and C_{12b}.

(b) The NQI is strong in one manifold and weak in the other. There will be curve with an internal extreme value along one axis, as observed in the case of C_{12a}.

(c) A weak NQI situation exists in both manifolds. The curve will have internal extreme values along both frequency axes, but, generally, the maxima will not occur simultaneously.

Only in case (c) is it possible to measure ω_{extr} from both manifolds simultaneously if the shape of the dq,dq peaks is resolved. The absolute value of the hyperfine constant a may be easily determined:

$$|a| = \left|\frac{\omega_{\mathrm{extr},\alpha}^2 - \omega_{\mathrm{extr},\beta}^2}{8\omega_I}\right| \quad (58)$$

The other quantity that can be determined is

$$\kappa^2(3+\eta^2) = \frac{\omega_+^2 + \omega_-^2}{8} - \frac{a^2}{4} - \omega_I^2 \qquad (59)$$

This relation allows us to estimate the quantity κ^2 within an accuracy of 25% when the value of η is unknown. Even when the shape of the ridge is poorly resolved, eqs 58 and 59 may be used to estimate the respective quantities from the extreme edges of the dq,dq peaks in the limit of purely isotropic HFI with weak quadrupoles. Figure 3 illustrates the variation of the C_{22c} ZWR on the asymmetry of the quadrupole interaction in the weak quadrupole case.

Let us examine the case of high asymmetry in the quadrupole interaction when $\eta = 1$. In this case, the weak quadrupole condition (eq 30) is valid, regardless of the value of the quadrupole coupling constant κ. The range of values for parameter f is now symmetric: $-2 \le f \le 2$. As mentioned previously, the maximum values of the double quantum frequencies in both manifolds occur in the middle of this range (see eq 31) when $f = 0$. It is easily shown that, in this particular case, $\xi_{m,1}(f) = \xi_{m,1}(-f)$. This means that the two branches of the C_{22} ridge for $\pm f$ coincide (see also Figure 3 for illustration) and the ridge, as a whole, has a C_{11}-type appearance. One important relation is also valid in this case: $\xi_{m,2}(f) = -\xi_{m,3}(-f)$. The ridges that correlate single quantum transitions now coincide. The total number of ridges in the two quadrants is 20 instead of 36 in this case.

Figure 4 displays the spatial relationships for the different types of peaks and ridges in the frequency plane in the case of isotropic HFI. Because of the symmetry of the HYSCORE spectra, usually only the positive values of ω_2 are presented. It is important to note that the C_{22}-type ridges may appear only in four small rectangles, which are positioned symmetrically, with respect to the ω_2-axis. The maximum size of these rectangles may be defined using relation 27, so that, in the positive quadrant,

$$\sqrt{3|p_\alpha|} \le \omega_1 \le 2\sqrt{|p_\alpha|} \qquad (60a)$$

$$\sqrt{3|p_\beta|} \le \omega_2 \le 2\sqrt{|p_\beta|} \qquad (60b)$$

$$\sqrt{3|p_\beta|} \le \omega_1 \le 2\sqrt{|p_\beta|} \qquad (60c)$$

$$\sqrt{3|p_\alpha|} \le \omega_2 \le 2\sqrt{|p_\alpha|} \qquad (60d)$$

These dq peaks are often prominent features of the spectra. Equations 58 and 59 can be used to measure the isotropic HFIs and quadrupole interactions when the weak quadrupole condition applies, and ω_{extr} can be identified in both electron spin manifolds. This can be prevented by poor resolution, or "blind spots" from the variation of spectral intensity with τ or the strong quadrupole condition. Even then, relation 60 shows that eq 58 may be used to estimate the hyperfine constant value with at least 25% accuracy, whereas eq 59 allows estimation of the quadrupole splitting with less accuracy. Figure 3 shows that C_{22} may extend over only a small fraction of its allowed range. Equations 58−60 determine the possible range of parameters for numerical simulation of the spectra, to further refine parameters. The double quantum frequencies, as measured from dq,dq or dq,sq correlation ridges, must obey eq 60 and Figure 4 if the HFI is purely isotropic. Thus, these relations are a necessary condition for experimental HYSCORE spectra, to apply the analysis methods presented here.

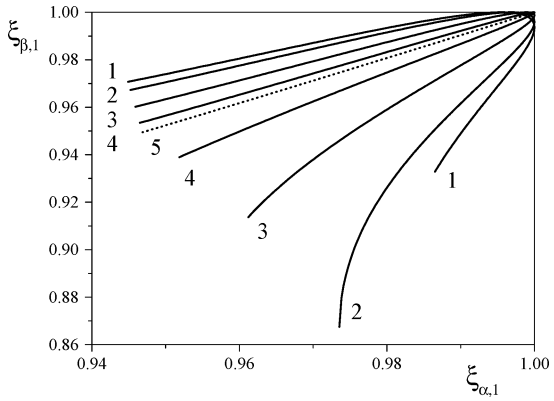

Figure 3. Dependence of the dq,dq zero width ridge (ZWR) on the asymmetry of the quadrupole interaction in the case of weak quadrupole interaction C_{22c}. The values of the parameters are as follows: $\omega_I = 1$; $a = 1$; $\kappa = 0.3$; and $\eta = 0$ (for curve 1), 0.4 (for curve 2), 0.7 (for curve 3), 0.9 (for curve 4), and 1 (for curve 5). In the case of $\eta = 1$ (the dotted curve), the two branches of the ridge coincide.

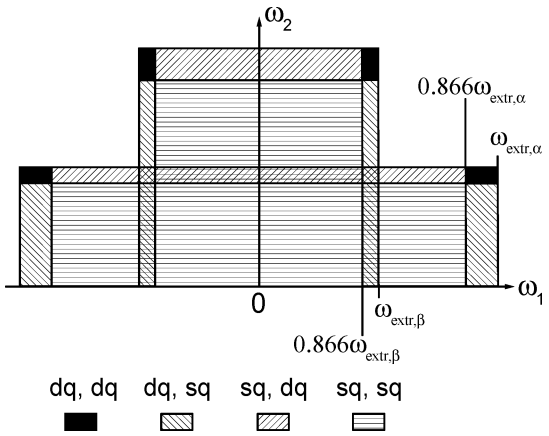

Figure 4. Location of different types of correlation ridges in the HYSCORE spectrum from $I = 1$ with arbitrary nuclear quadrupole interactions (NQIs) and isotropic hyperfine interactions (HFIs). These regions are useful for assigning ridges to particular types of transitions, because only a small overlap or regions is allowed for dq,sq or sq,dq correlations with regions of sq,sq correlations, as indicated by the overlapping cross-hatched regions.

The Supporting Information contains an atlas of HYSCORE spectra of an orientationally disordered system, as a function of the dimensionless parameters $a' = a/\omega_I$, $\kappa' = \kappa/\omega_I$, and η. To reduce the number of parameters, the short τ approximation (eq 9) was used for the intensity calculations. Each ZWR is presented as a set of 50 circles. The centers of these circles are taken at equidistant values of parameter f, whereas their diameters are proportional to the spectral intensity at this point. Their color denotes the sign of the intensity: red for positive values, blue for negative values. Note that, because of the symmetry of the Hamiltonian (eq 23), the substitution $\{a' \Rightarrow 4/a', \kappa' \Rightarrow 2\kappa'/a'\}$ gives the same pattern but with a different frequency scale and intensity distribution.

Experimental Section

EPR. A 10 mM sample of the ethylenediaminetetraacetic acid (EDTA) complex of oxovanadium (VO(II)−EDTA) in a 30% glycerol:H_2O solution was prepared from a VO(II) sulfate in a Wilmad model 707-SQ 4-mm-outer diameter (OD) EPR sample tube, as described by Dikanov et al.[16]

EPR measurements were made on a Bruker model ESP380E pulsed EPR/ENDOR spectrometer with an X-band Flexline

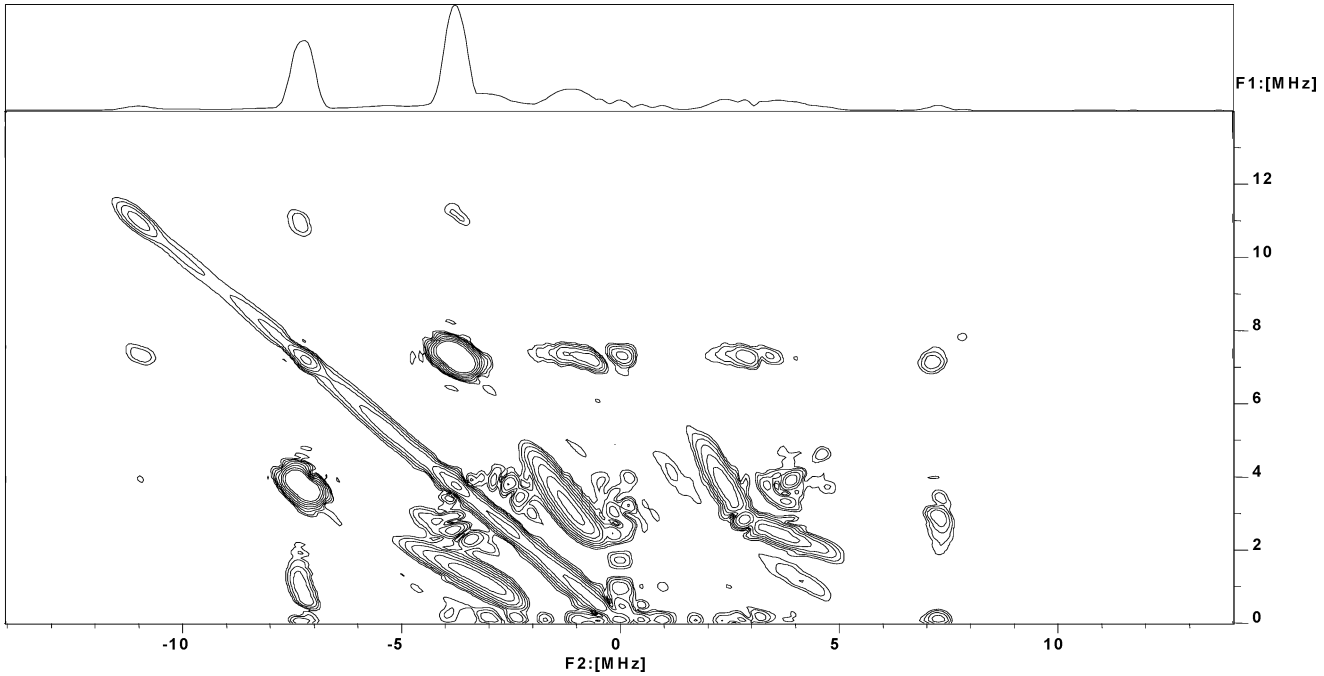

Figure 5. Low-frequency region of the HYSCORE spectrum of 10 mM oxovanadium−EDTA complex in a mixture of water and glycerol at 30 K with $\tau = 168$ ns, showing the correlations of the ^{14}N atom. The contours are logarithmically spaced to reveal the shape of the extended correlation ridges. The highest contour is set well below the amplitude of the intense dq,dq correlation peaks. A so-called "skyline projection" of the two-dimensional (2-D) spectrum is shown at the top of the figure.

ENDOR resonator and a cryostat with an Oxford model ITC-503 temperature controller. Measurements were made at a temperature of 30 K with a magnetic field of 344.4 mT, which corresponded to the maximum absorption peak at the $m_I^V = -1/2$ line of the VO(II) complex with EDTA. The standard HYSCORE pulse sequence was used with nominal pulse widths of 16 and 24 ns for the $\pi/2$ and π pulses, respectively. Unwanted echoes were suppressed by phase cycling. A 256 × 256 dataset was recorded with times t_1 and t_2 incremented in 16-ns steps from initial values of 48 and 32 ns, respectively, with $\tau = 168$ ns at a pulse repetition rate of 997 Hz.

Spectral Processing. The HYSCORE datasets were processed using the 2-D WIN-EPR software package from Bruker. Contour lines are drawn at logarithmically spaced intervals, and "skyline" projections of the 2-D spectra are shown.

Results

VO−EDTA was chosen to illustrate our treatment of HYSCORE for several reasons: (i) the oxovanadium ion has two equivalent nitrogens as direct ligands; (ii) the nitrogens have a HFI that seems to be completely isotropic; (iii) this complex has one region in its spectrum (the $m_I^V = -1/2$ vanadium hyperfine line), where almost all orientations of the complex are simultaneously resonant at the X-band, minimizing complications from unintended orientation selection); and (iv) this complex is a spectroscopic model for oxovanadium complexes that can be formed with biological molecules and proteins. This brief example illustrates the application of the quantitative relations developed earlier for the analysis of HYSCORE spectra of $I = 1$ nuclei when the hyperfine coupling is isotropic. It also demonstrates how both the size and location of regions in Figure 4 can be used to assign spectral features and how they can be used as necessary conditions for accepting that the hyperfine coupling is isotropic.

The low-frequency region of the HYSCORE spectrum is shown in Figure 5. The diagonal ridge on the left-hand (+, −) quadrant of the spectrum is an artifact that occurs when there is insufficient time for total relaxation of spins between repetitions of the pulse sequence. There are also a few weak peaks where at least one frequency has a magnitude of >8 MHz. These peaks result from combinations of frequencies from the two nitrogens in the complex and are consistent with predictions of the so-called "product rule".

By far, the most intense peaks are a pair of sharp lines at (+7.4, −3.9) and (+3.9, −7.4), abbreviated here as [±7.4, ∓3.9]. They are so intense that the tops of the peaks are well above the highest contour line and only the base of the peak is indicated by the contour lines. However, their full intensity is visible in the skyline projection at the top of the figure. These are the dq,dq correlation peaks. Their line shape is approximately Gaussian, as determined by the apodization function used on the 4 μs × 4 μs dataset. Other major ridges include dq,sq correlations at [±7.4, ∓1] and [7.4, 3], as well as sq,sq correlations at [±3, ∓1], [4, 2] and a weaker pair at [4, 1].

The experimental spectra resemble the general shape of calculated spectra for $a = 4\omega_I$, $\kappa = (0.5-1.0)\omega_I$ in the Supporting Information. A few calculated spectra are reproduced in Figure 6. One must remember that interference effects and the so-called "τ suppression effect" in the experimental spectra may prevent observation of all the ridges that have been calculated for the small τ limit in the Supporting Information. The significant features are that (i) the coordinates for the dq,dq peaks have an approximate ratio of 2:1; (ii) the dq,sq ridges show considerable overlap; and (iii) the sq,sq ridges are tilted slightly from either the diagonal or "anti-diagonal".

The full width of the dq,dq peaks at the baseline are significantly broadened by the apodization of the limited dataset that was recorded. The dq,dq peaks are within the range of 6.9−7.6 MHz in one dimension and 3.4−4.2 MHz in the other. The peak widths in both dimensions, after considering that these are baseline-to-baseline widths and that there is significant

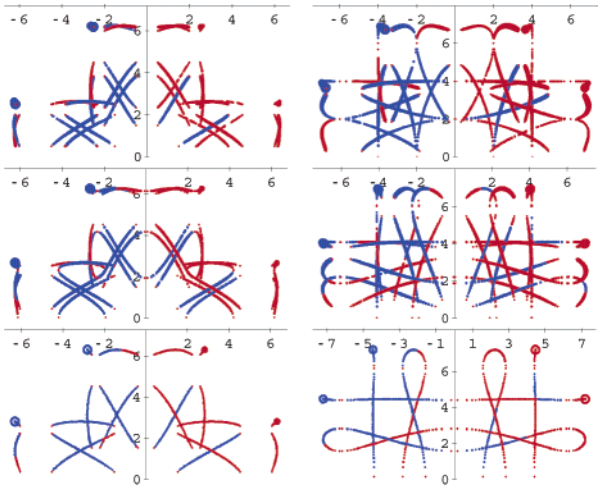

Figure 6. Numerically calculated spectra that are similar to the experimental spectrum shown in Figure 5. The peak intensities shown here are proportional to the area of the circles (in the Supporting Information, where pictures are presented in a scalable form, intensities are proportional to the radii). The values of parameters are as follows: $a = 4\omega_I$; $\kappa = 0.5\omega_I$ (left column); $\kappa = \omega_I$ (right column); and $\eta = 0.001$, 0.5, and 0.999 for the first, second, and third rows, respectively. The last row illustrates that some ridges coincide when $\eta \rightarrow 1$.

experimental broadening, are within the limits for dq,dq peaks that have been described previously and in Figure 4. The widths or positions of the dq,dq peaks did not change in HYSCORE spectra that were obtained at other values of τ. Also, HYSCORE spectra measured at other positions in the EPR spectrum showed the shifts that were expected from the change in magnetic field but did not exhibit any of the properties of an anisotropic HFI measured under orientation selection conditions. All indications are that the hyperfine coupling is completely isotropic. In addition, the dq,sq and sq,sq ridges seem to have the same constant width, as expected of ZWRs with apodization.

The very rough hyperfine and quadrupole estimates that were made from the spectral atlas place this spectrum well within the weak quadrupole limit. Thus, the maximum magnitudes of the double quantum frequencies correspond to ω_{extr} in both dimensions, because the hyperfine coupling is isotropic. However, the experimental broadening causes the peak rather than the edge to be a better estimate of the ω_{extr}. That gives ν_{extr} values ($\nu_{extr} = \omega_{extr}/2\pi$) of 3.78 ± 0.1 and 7.3 ± 0.1 MHz, which correspond to $p_{\alpha/\beta}$ values of −3.6 ± 0.2 and −13.3 ± 0.2 MHz^2, giving an isotropic hyperfine coupling of 4.58 ± 0.05 MHz and $\kappa^2(3 + \eta^2) = 2.08 \pm 0.05$ MHz^2. The latter relation leads to the estimation 0.72 MHz $< |\kappa| <$ 0.83 MHz.

The value of ω_{extr} can also be measured from the dq,sq correlation ridge near [±7.4, ∓1]. Because the weak quadrupole condition is met, this is a C_{12A} ridge, whose maximum frequency of 7.38 MHz along the center of its ridge is equal to ω_{extr} and agrees well with the value obtained from the dq,dq peak.

Conclusions

The hyperfine sublevel correlation (HYSCORE) spectra of paramagnetic centers that have electron spin $S = {}^1/_2$ and nuclear spin $I = 1$ in the presence of isotropic hyperfine interactions (HFIs) and nuclear quadrupolar interactions (NQIs) of arbitrary strength have been explicitly considered. The HYSCORE spectrum, under these conditions, is a set of 36 ridges that have zero width. An analytical expression in parametric form for the location and intensity of these ridges is derived and is useful either for simulating spectra or for understanding their general features. Ridges for the different types of HYSCORE correlations (the dq,dq or dq,sq or sq,sq correlations, where dq denotes double quantum and sq denotes single quantum) are found in strictly delineated regions of the spectrum, when the HFI is isotropic. This aids both in the assignment of ridges to specific types of transitions and in the rapid estimation of hyperfine and quadrupole coupling constants. The application of these results was illustrated on a HYSCORE spectrum obtained from the ethylenediaminetetraacetic acid (EDTA) complex of oxovanadium. An atlas of simulated spectra in the Supporting Information is provided for a broad range of isotropic hyperfine and quadrupole couplings, for comparison with experimental spectra.

The particular case of $I = 1$ with isotropic hyperfine and arbitrary quadrupoles treated in detail here does have some practical importance. We have observed HYSCORE spectra that seem to have isotropic nitrogen HFI with sharp dq,dq correlations and well-resolved dq,sq and sq,sq zero width ridges (ZWRs), reminiscent of Figure 5 in several classes of samples. These include oxovanadium complexes of nitrogen-containing ligands, such as the EDTA illustrated here and histidine,[16] several metalloproteins and oxovanadium complexes of proteins, and small nitrogen-containing molecules adsorbed onto activated metal oxide surfaces. The results obtained here are aiding in their detailed interpretation.

In addition, the exact results obtained here for isotropic HFI provide a good starting point for addressing the more-difficult problem of arbitrary HFIs. It is more complicated in two ways. First, the frequencies are no longer a function of the single orientational parameter f, but, instead, are dependent on two parameters. As a result, the ridges no longer have zero width but have a two-dimensional shape, with the added complication that a transition frequency in one electron spin manifold does not map onto a single frequency in the other manifold but rather onto a range of frequencies. Consequently, the equations for the shapes of the ridges are much more complicated. Second, the number of degrees of freedom is greater. Instead of the quadrupole coupling constant, its asymmetry, and a single hyperfine coupling, there are the quadrupole coupling constant, its asymmetry, three anisotropic hyperfine coupling constants, and the three Euler angles relating the quadrupole and hyperfine axis systems. Identifying the key spectral features, analogous to ω_{extr} that would allow rapid estimation of the spin Hamiltonian parameters, is much more difficult in the general case. However, the results for isotropic hyperfine couplings provide a valuable starting point for the treatment of weak hyperfine anisotropy, such as that observed in the histidine ligands to the Rieske iron sulfur clusters[3] or for weakly coupled deuterons.

During the development of these specific results for $I = 1$ with isotropic HFIs, three important results of much greater applicability were observed:

(1) The vector formalism developed previously[13] to describe electron spin−echo envelope modulation (ESEEM) for one-, two-, and three-pulse sequences was extended to describe HYSCORE spectra. This formalism provides a compact description that applies to any nuclear spin and to any arbitrary HFI or quadrupole interactions.

(2) The form of the HYSCORE spectrum in the limit of small τ was developed. When τ is small—that is, much smaller than the period of the largest frequency in the spectrum—the intensity of the spectrum then scales with τ; however, the relative intensities of the different peaks do not change. This feature makes the short τ limit very useful for both theoretical and numerical HYSCORE simulations, because it provides an accessible standard set of conditions for comparing different

simulations and it is free of the so-called "τ-suppression effect" that can cause some HYSCORE features to disappear in spectra that have been measured or simulated at larger values of τ.

(3) A new method of calculating HYSCORE modulation (or any other ESEEM) was developed that uses only the spin Hamiltonian and the eigenvalues but does not require calculation of eigenvectors or the Mims matrix *M*. This method is based on the Cayley−Hamilton theorem and is applicable to any value of nuclear spin *I* with arbitrary HFI and quadrupole interactions. In addition, it simplifies integration over different orientations to give powder spectra.

Acknowledgment. This work was supported by the National Institutes of Health (under GM61904). The W. R. Wiley Environmental Molecular Sciences Laboratory is a national scientific user facility sponsored by the Department of Energy's Office of Biological and Environmental Research, and it is located at Pacific Northwest National Laboratory. A.G.M. acknowledges the Battelle Memorial Institute for a fellowship.

Supporting Information Available: Collection of two-dimensional HYSCORE spectra for paramagnetic ceenters with isotropic hyperfine interactions (HFIs) and a nuclear spin of $I = 1$, using short τ approximation (PDF). This material is available free of charge via the Internet at http://pubs.acs.org.

References and Notes

(1) Dikanov, S. A.; Tsvetkov, Yu. D. *Electron Spin Echo Envelope Modulation (ESEEM) Spectroscopy*; CRC Press: Boca Raton, FL, 1992.

(2) Schweiger, A.; Jeschke, G. *Principles of Pulse Electron Paramagnetic Resonance*; University Press: Oxford, U.K., 2001.

(3) Dikanov, S. A.; Xun, L.; Karpiel, A. B.; Tyryshkin, A. M.; Bowman, M. K. *J. Am. Chem. Soc.* **1996**, *118*, 8408.

(4) Dikanov, S. A.; Bowman, M. K. *J. Magn. Reson. A* **1995**, *116*, 125.

(5) Dikanov, S. A.; Tyryshkin, A. M.; Bowman, M. K. *J. Magn. Reson.* **2000**, *144*, 228.

(6) Magliozzo, R. S.; Peisach J. *Biochemistry* **1993**, *32*, 8446.

(7) Madi, Z. L.; Van Doorslaer, S.; Schweiger, A. *J. Magn. Reson.* **2002**, *154*, 181.

(8) Deligiannakis, Y.; Louloudi, M.; Hadjiliadis, N. *Coord. Chem. Rev.* **2000**, *204*, 1.

(9) Muha, G. M. *J. Chem. Phys.* **1980**, *73*, 4139.

(10) Muha, G. M. *J. Magn. Reson.* **1982**, *49*, 431.

(11) Broida, J. G.; Williamson, S. G. *Comprehensive Introduction to Linear Algebra*; Addison−Wesley: Reading, MA, 1989.

(12) Harris, W. A., Jr.; Fillmore, J. P.; Smith, D. R. *SIAM Rev.* **2001**, *43*, 694.

(13) Maryasov, A. G.; Bowman, M. K.; Tsvetkov, Yu. D. *Appl. Magn. Reson.* **2002**, *23*, 211.

(14) Bowman, M. K.; Massoth, R. J. Nuclear Spin Eigenvalues and Eigenvectors in Electron Spin−Echo Modulation. In *Electron Magnetic Resonance of the Solid State*; Weil, J. A., Bowman, M. K., Morton, J. R., Preston, K. F., Eds.; Canadian Society for Chemistry: Ottawa, Canada; pp 99−110.

(15) Maryasov, A. G. *Appl. Magn. Reson.* **2001**, *21*, 79.

(16) Dikanov, S. A.; Samoilova, R. I.; Smieja, J. A.; Bowman, M. K. *J. Am. Chem. Soc.* **1995**, *117*, 10579.